EVENTS DETECTABILITY IN NORTH AFRICA AND MIDDLE EAST BY THE INTERNATIONAL MONITORING SYSTEM INFRASOUND STATIONS

Hani. S. ELBEHIRI[1,2], Ibrahim KORAT[3], Ahmed LETHY[2], Masa-yuki YAMAMOTO[1]
Kochi University of Technology[1], Japan
National Research Institute of Astronomy and Geophysics [2], Egypt
Mansoura University[3], Egypt

***ABSTRACT*:** The infrasound wave is a type of low-frequency wave (less than 20 Hz). Furthermore, it propagates for long distances through the atmospheric layers with a velocity of ~ 343 m/s at 20° C without considerable attenuation. The International Monitoring System (IMS) infrasound stations are established for monitoring nuclear explosions in the atmosphere. Nowadays, the IMS infrasound network contains 53 certified stations out of 60 planned to be constructed. Data from seven IMS infrasound stations around Africa for a period between the 1st of January 2013 and the 21th of April 2018 is used in this study to estimate the detectability of events around Africa and the Middle East with data availability of more than 99.2%. The Progressive Multichannel Cross-Correlation (PMCC) algorithm developed by the Commissariat à l'Energie Atomique (CEA) (French Atomic Energy Commission) is used with 11 frequency bands for the data processing. These bands start at an extremely low frequency of 0.07 Hz and end at 4 Hz. In addition, Statistical analysis for this period is produced for qualitative and quantitative description using the Dase Tool Kit (Détections Infrasons Valorisées Automatiquement) (DTK-DIVA) software. The stations show a clear difference in detection numbers between day and night hours as the detections in the day hours are less than the night at all stations except at the Germany I26DE station, which has no noticeable diurnal difference being attributed to climatic and meteorological factors as most of the stations have tropical and dry climates except for this station, which has a temperate oceanic climate. Additionally, there is a vital relationship between seasons and the number of detections, as infrasound waves are affected by climate change.

KEYWORDS: Infrasound, Atmosphere, Detections

1. INTRODUCTION

Infrasound waves are a type of low-frequency sound waves that have frequencies lower than the bottom limit of human audibility with a range from 0.003 to 20 Hz [1]. Its propagation is strongly dependent on the temperature and wind structure of the atmosphere [2]. It travels from its source through the atmosphere with ~343 m/s at 20° C [3, 4]. These waves can travel thousands of kilometers through the atmosphere without considerable attenuation. Infrasonic waves are produced by many natural and manufactured sources. Natural sources include volcanoes, meteorites, large earthquakes, thunderstorms, microbaroms, and avalanches. Manufactured sources include mining and chemical blasts, nuclear explosions, wind turbines, drones, helicopters, and rocket launches [5–7]. The IMS is a part of the Comprehensive Test Ban Treaty (CTBT) verification regime [8, 9]. The IMS stations with

their four categories; seismic, infrasound, hydro-acoustic, and radionuclide monitor the world for any nuclear explosion worldwide in the solid earth, atmosphere, and oceans. IMS infrasound stations are distributed to detect explosions in the atmosphere with a yield equivalent to 1 kiloton of TNT by at least two stations [10]. Studying the infrasound station detectability requires analysis of data for a long time.

1.1 Data Set and the Study Area

Seven infrasound IMS stations surround the research area and are used to study the event's detectability in North Africa. These stations are I17CI, I19DJ, I26DE, I31KZ, I32KE, I43RU, and T48TN. The Cote d'Ivoire I17CI station is considered the farthest one, with a distance to the nearest study point of about 3200 km. This distance is not considered a long one because infrasound waves travel through continents without considerable attenuation. These stations could cover the northern part of Africa including the study area (latitudes ~20-40° N and longitudes ~20-40° E). The used data is from 1st January 2013 to 21th April 2018 (five years, three months, and three weeks). Additionally, data availability statistics are generated to estimate the status of stations during the study period. Figure 1 shows the data availability study. It showed that, during this period, the average data availability was very high as it attained 99.29%. Figure 2 shows the study area and the location of the stations.

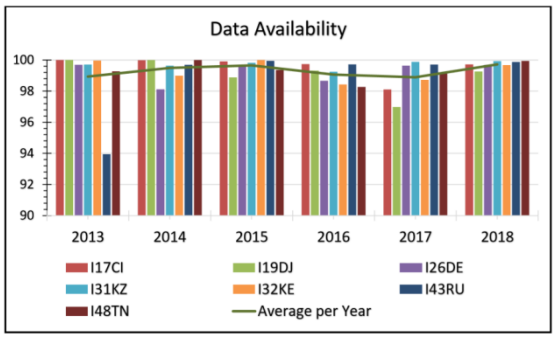

Figure 1 Data availability histogram.

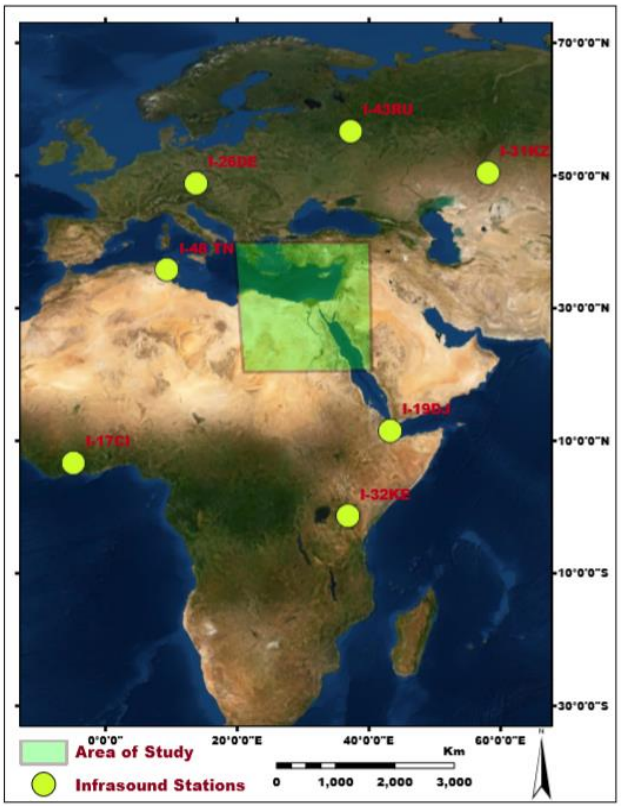

Figure 2 The study area (green rectangular) and the surrounding seven infrasound IMS stations.

2. METHODOLOGY

The PMCC algorithm is the base of the infrasound data processing method [11–13]. By supposing the spectral amplitude is A(f), the signal phase is φ(f) in the Fourier transform (Equation 1) that represents the signal in the frequency domain instead of the time domain.

$$S(t) = \int_{-\infty}^{\infty} A(f) e^{i\emptyset(f)} df \qquad (1)$$

By supposing a plane wave that propagates through several sensors that are distributed as an array, the variation in amplitude and phase between two sensors in the array is considered the background noise. In the ideal state without any background noise at different sensors, Equations 2 and 3 represent the detections of the signal by assuming three sensors in the array that have (i, j, and k) positions.

$$A_j(f) = A_i(f) \quad (2)$$

$$\varphi_j(f) = \varphi_i(f) - \Theta\,(\vec{r}_j - \vec{r}_i) \quad (3)$$

The vector of the sensor position is represented with $\vec{r}$. By cross-correlation between two sensors in the array, the delay of wave arrival could be measured from the variation in the atmospheric pressure. The delay in wave arrival time between two sensors at positions i and j can be defined as Δt_{ij} which represents the only difference between the data recorded by the two sensors[14]. This phase delay depends on three parameters; the sensor position $\Theta.(\vec{r}_j - \vec{r}_i)$, trace velocity and the wave incident azimuth. The delay in time value for the record between any two elements in the array Δt can be calculated from Equation 4.

$$\Delta t_{ij} = \frac{1}{2\pi f}\,(\varphi_{j(f)} - \varphi_{i(f)}) \quad (4)$$

For the planner wave that propagates through elements i, j, and k of an array, the sum of the delays in wave detection between every two sensors should be zero in case of neglecting the background noise. This relation is the closure one which can be represented in Equation 5.

$$\Delta t_{ij} + \Delta t_{jk} + \Delta t_{ki} = 0 \quad (5)$$

If background noise is present within the wave propagating through an array of elements the sum of delays between elements is not exactly zero and the accuracy of the cross-correlation operation decreases. The algorithm is progressively applied, and the consistency value is calculated from the following relation.

$$Cn = \sqrt{\frac{6}{n\,(n-1)(n-2)}\,r_{ijk}^2} \quad (6)$$

C_n is the consistency value, n is the number of elements, and r_{ijk} is the sum of delays between elements i, j, and k belonging to the array (R_n). The consistency value is calculated firstly from the delays between the smallest sub-elements triangle. If the consistency value is below the given threshold, the detection is stated [15].

2.1 Detection Parameters

The International Data Center (IDC) parameters with the eleven frequency bands are selected for processing the data. These bands start at an extremely low frequency of 0.07 Hz and end at 4 Hz. Each frequency band has a different window length with an overlap percentage value. A long window length with a high-overlap percentage is used with the low-frequency band. Infinite impulse response filters are used by the PMCC software fitted with Chebyshev filters of orders 2 and 3 and ripples varying between 0.005 to 0.1. These parameters contribute to the source classification and location. Table 1 has a brief description of all frequency bands.

Table 1 Eleven frequency bands with the detection parameters.

F(min)	F(max)	Window Length (s)	Overlap (%)	Filter type	Order	Ripple (dB)
0.07	0.1	60	83.3	Chebyshev I	3	0.01
0.1	0.2	60	83.3	Chebyshev I	3	0.01
0.2	0.35	60	83.3	Chebyshev I	3	0.01
0.35	0.5	50	80	Chebyshev I	3	0.005
0.5	0.7	50	80	Chebyshev I	2	0.02
0.7	0.9	50	80	Chebyshev I	2	0.02
0.9	1.2	50	80	Chebyshev I	2	0.02
1.2	1.6	50	80	Chebyshev I	2	0.02
1.6	2.2	40	75	Chebyshev I	2	0.02
2.2	3	40	75	Chebyshev I	2	0.1
3	4	30	66.6	Chebyshev I	2	0.1

3. RESULTS

The statistical analysis applied to the seven stations surrounding the study area gives the quantitative manner of their detections and an inverse qualitative

description of the atmospheric state as wind directions.

3.1 Diurnal Variation

Detectability study of the stations shows an obvious difference in number between day and night hours (day/night property). This property could be attributed to the influence of solar radiation which was also detected in an experiment in Norway[16]. Figure 3 shows a pie plot for all stations in this study summarizing the diurnal variations in detection numbers.

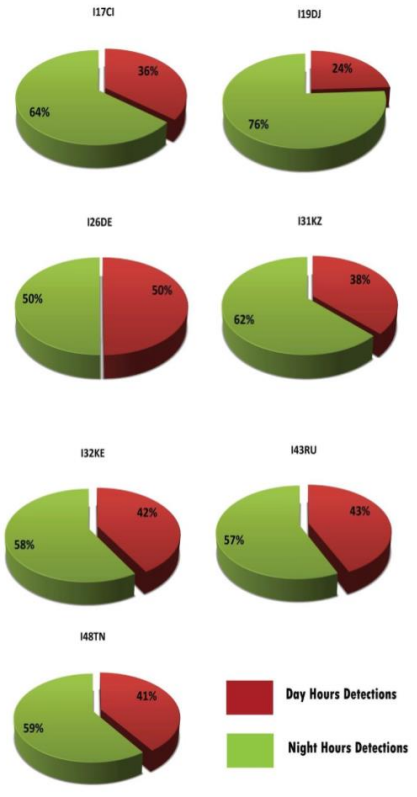

Figure 3 Comparison between day and nightdetection percentages.

The number of whole detections during day hours is lower compared with that during the night hours at all stations except Germany I26DE station which has no noticeable day/night variation. The stability in its detections might be argued to be climatic and meteorological factors as this station has a temperate oceanic climate, while most other stations have tropical and arid climates. Table 2 summarizes the classification of the climate at each station according to the Köppen-Geiger climate classification system [17].

Table 2 Climatic classifications at all stations.

Station	Climate Classification
I17CI	dry tropical climate
I19DJ	Tropical and Subtropical Desert Climate
I26DE	Temperate oceanic climate
I31KZ	forest-steppe, steppe, semi-arid, and desert climate zones
I32KE	equator and has a pleasant, tropical climate
I43RU	Due to the huge size of the country, Russia has almost all climate zones in the world
I48TN	hot-summer Mediterranean climate

3.2 Seasonal Variation and Source Classification

The infrasound wave is affected by temperature and climatic changes; therefore, the detection numbers vary with different seasons. All stations showed a seasonal variation for various sources as shown in the following station I17CI. Initially, the detections at the study station are attributed to various sources such as thunderstorms and local events with frequencies up to 5 Hz from different back-azimuths. In addition to microbaroms detected from oceanic waves specifically the Atlantic Ocean. Some of these sources are detected seasonally and others continuously. Microbarom detections with low frequency ranging between 0.01 to 0.5 Hz had been analyzed to show seasonal variation in this station. Figure 4 shows seasonal variation in I17CI stations specifically for microbaroms.

Microbarom detections are distributed in various azimuths representing wind direction; especially from the southeast between 105-140˚, from the south 160-220˚, and the west extending to northwest 230-350˚. These microbarom detections are from the

Atlantic Ocean surrounding the Côte d'Ivoire station, from northeast to south directions, and from the southeast at the Gulf of Guinea. In Figure 4, The detections between 105-140˚ show seasonal variations as they appear in summer from mid-May to the end of August. Additionally, detections from the south between azimuths 160-220˚ witness seasonal increase in the warm season; spring and summer months from mid-April to the end of September. On the other hand, in the dry-hot season; from mid-November to mid-May, witness the microbaroms detections that come from the west and the northwest (between 230-350˚).

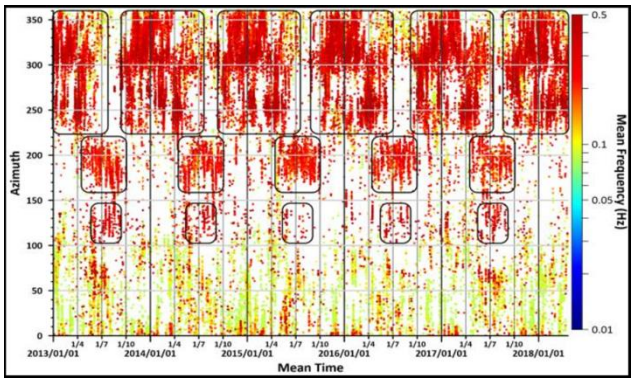

Figure 4 Scattering plot of detection showing the seasonal variation of microbaroms (I17CI station).

The second set from 0.5 to 5 Hz is represented in Figure 5 which contains high-frequency detections from sources such as thunderstorms and local artificial sources that also show seasonal variation. Figure 5 shows three clusters. The first has continuous detections all over the year near azimuth between 80 to 120˚. The second cluster is around azimuth ~150˚ with two occurrence periods from June to October and from December to the end of February. Finally, the detections from the west and northwest with azimuths between 220 and 350˚ Also have two occurrence periods; between March and mid-June and September to end-November. Not only does I17CI contain seasonal variation for the events but also all stations.

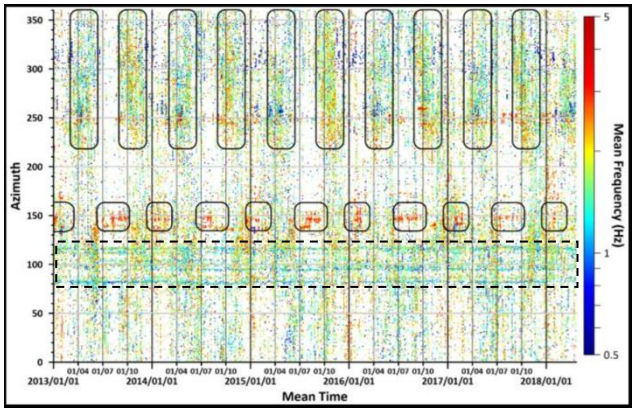

Figure 5 Scattering plot of detection showing seasonal variation detections with a frequency between 0.5 to 5 Hz (I17CI station).

4. CONCLUSION

In conclusion, detections at all stations have both diurnal and seasonal variability. They have a higher probability during night hours than during day hours. Day and night change in detectability is attributed to solar radiation taking into consideration the climate change in different stations. The infrasound detections are seasonally dependent with the same cycles per year for those with frequency content less than 0.5 Hz which are microbaroms, and also for the high-frequency ones in I17CI station. Not only does the I17CI station show seasonal variation for various sources, but also all stations in the region.

REFERENCES

[1] K. Kyriakides and H. G. Leventhall, "Some effects of infrasound on task performance," *J. Sound Vib.*, vol. 50, no. 3, pp. 369–388, 1977, doi: 10.1016/0022-460X(77)90490-4.

[2] T. M. Georges, W. H. Beasley, T. M. Georges, and W. H. Beasley, "Refraction of infrasound by upper-atmospheric winds," *ASAJ*, vol. 61, no. 1, pp. 28–34, 1977, doi: 10.1121/1.381263.

[3] L. G. Evers and H. W. Haak, "The characteristics of infrasound, its propagation and some early history," *Infrasound Monit.*

Atmos. Stud., pp. 3–27, 2009, doi: 10.1007/978-1-4020-9508-5_1.

[4] M. N. ElGabry, I. M. Korrat, H. M. Hussein, and I. H. Hamama, "Infrasound detection of meteors," *NRIAG J. Astron. Geophys.*, vol. 6, no. 1, pp. 68–80, Jun. 2017, doi: 10.1016/J.NRJAG.2017.04.004.

[5] P. Campus and D. R. Christie, "Worldwide observations of infrasonic waves," in *Infrasound Monitoring for Atmospheric Studies*, Springer Netherlands, 2009, pp. 185–234.

[6] J. Park, S. J. Arrowsmith, C. Hayward, B. W. Stump, and P. Blom, "Automatic infrasound detection and location of sources in the western United States," *J. Geophys. Res. Atmos.*, vol. 119, no. 13, pp. 7773–7798, Jul. 2014, doi: 10.1002/2013JD021084.

[7] I. Hamama *et al.*, "Investigation of near-surface chemical explosions effects using seismo-acoustic and synthetic aperture radar analyses," *J. Acoust. Soc. Am.*, vol. 151, no. 3, p. 1575, Mar. 2022, doi: 10.1121/10.0009406.

[8] S. J. Arrowsmith, "False alarms and the IMS infrasound network: Understanding the factors influencing the creation of false events," *Geophys. J. Int.*, vol. 215, no. 2, pp. 1322–1337, 2018, doi: 10.1093/GJI/GGY350.

[9] A. Agrebi, A. H. Ramanantsoa, G. Rambolamanana, and E. H. Rasolomanana, "Characterisation of the Coherent Infrasound Sources Recorded by the Infrasound International Monitoring System Station I48TN in Tunisia (Mines & Quarries)," *Atmos. Clim. Sci.*, vol. 11, no. 01, pp. 214–243, 2021, doi: 10.4236/ACS.2021.111014.

[10] D. R. Christie *et al.*, "Detection of atmospheric nuclear explosions: the infrasound component of the International Monitoring System," *Kerntechnik (1987)*, vol. 66, no. 3, pp. 96–101, 2001, Accessed: Jan. 07, 2022. [Online]. Available: http://inis.iaea.org/Search/search.aspx?orig_q=RN:32036541.

[11] Y. Cansi, "An automatic seismic event processing for detection and location: The P.M.C.C. Method," *Geophys. Res. Lett.*, vol. 22, no. 9, 1995, doi: 10.1029/95GL00468.

[12] Y. Cansi and Y. Klinger, "(1) (PDF) An automated data processing method for mini-arrays," 1997. https://www.researchgate.net/publication/237698457_An_automated_data_processing_method_for_mini-arrays (accessed Apr. 17, 2021).

[13] A. Le Pichon and Y. Cansi, "Le Pichon, A. and Cansi, Y. (2003) PMCC for Infrasound Data Processing. InfraMatics, 2, 1-9. - References - Scientific Research Publishing," 2003. https://www.scirp.org/(S(czeh2tfqyw2orz553k1w0r45))/reference/ReferencesPapers.aspx?ReferenceID=1366620 (accessed Feb. 06, 2021).

[14] I. Hamama and M. Y. Yamamoto, "Infrasonic earthquake detectability investigated in southern part of Japan, 2019," *Sensors (Switzerland)*, vol. 21, no. 3, pp. 1–16, 2021, doi: 10.3390/s21030894.

[15] Y. Cansi and A. Le Pichon, "Infrasound Event Detection Using the Progressive Multi-Channel Correlation Algorithm," in *Handbook of Signal Processing in Acoustics*, Springer New York, 2008, pp. 1425–1435.

[16] L. G. Evers and J. Schweitzer, "A climatology of infrasound detections in northern Norway at the experimental ARCI array," *J. Seismol.*, vol. 15, no. 3, pp. 473–

486, Jul. 2011, doi: 10.1007/S10950-011-9237-8.

[17] M. C. Peel, B. L. Finlayson, and T. A. McMahon, “Updated world map of the Köppen-Geiger climate classification,” *Hydrol. Earth Syst. Sci.*, vol. 11, no. 5, pp. 1633–1644, 2007, doi: 10.5194/HESS-11-1633-2007.